Electron-Spin Resonance of $K_2ZnF_4:Mn^{2+}$

V. J. Folen*
Naval Research Laboratory, Washington, D.C. 20390
(Received 10 April 1972)

Electron-spin-resonance (ESR) measurements at 24 GHz have been made on single crystals of K_2ZnF_4 doped with Mn. The spectra obtained in these measurements correspond to Mn^{2+} in the Zn^{2+} sites (point group $4/mmm$) in this material. The measured values of the spin-Hamiltonian parameters corresponding to the fine and hyperfine structure are $g_{\parallel}=2.0030$, $g_{\perp}=2.0028$, $A=-88.7\times10^{-4}$ cm^{-1}, $B=-89.3\times10^{-4}$ cm^{-1}, $D=36.0\times10^{-4}$ cm^{-1}, $a=5.6\times10^{-4}$ cm^{-1}, and $F=1.9\times10^{-4}$ cm^{-1}. In addition, the transferred hyperfine parameters were obtained from the ESR measurements. The measured values of these parameters, which result from interactions between the Mn^{2+} $3d$ electrons and F^- and which refer to the four equivalent nearest-neighbor F^- ions in the (001) plane (type I) and the two equivalent nearest-neighbor F^- ions along the fourfold axis (type II), are $A_s^{I}=18.1$, $A_s^{II}=14.9$, $A_\sigma^{I}=0.4$, $A_\sigma^{II}-\frac{1}{2}A_\pi^{II}=0.3$, and $A_\pi^{I}\approx0$, where the subscripts s, σ, and π refer to s, p_σ, and p_π electronic bonding, respectively, and all quantities are in units of 10^{-4} cm^{-1}. From these superhyperfine parameters, the fractions of unpaired spin densities were calculated.

I. INTRODUCTION

Since the discovery[1] of transferred hyperfine structure in the electron-spin resonance (ESR) of Ir ions in alkali choroplatinates, transferred hyperfine [or superhyperfine (shf)] structure has been observed[2] in a number of cubic fluorides and in a few noncubic fluorides. Some of these investigations have provided direct measurement of the properties of transition-metal-ion–ligand-ion bonding and have yielded important information on the overlap and covalent admixtures that must be present in order that the shf structure may exist. A knowledge of these admixtures is not only useful in theoretical investigations of bonding but it is also useful in the analyses of superexchange interactions and in the determination of the origin of magnetic properties of the transition-metal ions in ionic compounds. A typical example of such a property is the axial anisotropy of the transition-metal ions.

In the present work, the ESR spectra of Mn^{2+} in K_2ZnF_4 were investigated. In this material the Mn^{2+} ions replace the Zn^{2+} ions substitutionally and are present in sites having tetragonal symmetry. Thus, the Mn^{2+} ions possess a purely axial anisotropy with no complications arising from rhombic symmetry. In addition, because of the presence of F^- neighbors (for which there is 100% isotopic abundance having a nuclear spin of $\frac{1}{2}$), it was possible to determine transferred hyperfine interactions (THI) from the ESR. In contrast with the situation which exists when the paramagnetic ion is located at a site having a cubic point group, the presence of tetragonal symmetry permits the separation of the π-bonding contributions from the σ-bonding contributions to the shf tensor. Thus, in view of the fact that the Fermi contact term can normally be separated from the p_π and p_σ terms, all of the relevant shf tensor contributions can be separately and directly evaluated.

II. SINGLE-CRYSTAL SYNTHESIS AND CRYSTALLOGRAPHY

The single-crystal synthesis of K_2ZnF_4:Mn was accomplished by means of a flux technique. For this synthesis, 58 mole% of KHF_2, 42 mole% of ZnF_2, and 0.01 mole% of MnF_2 were dried under vacuum at 150 °C for 40 h and intimately mixed together with a mortar and pestle. The mixture was packed in a 40-ml platinum crucible and the crucible was loosely covered with a platinum cover. The crucible was then placed in an Al_2O_3 crucible with an Al_2O_3 cover. The latter crucible was fabricated to allow a flow of N_2 into its bottom so that a nonoxidizing atmosphere was maintained in the vicinity of the platinum crucible during the single-crystal synthesis. The double-crucible assembly was then placed into a furnace and heated slowly to 850 °C and maintained at this temperature for 1 h. The temperature was then lowered rapidly to 800 °C and held there for 1 h, and then lowered at the rate of 4 °C/h to 675 °C at which point it was lowered at an increased rate to 300 °C. The furnace power was turned off and after the single crystals cooled to room temperature they were removed from the flux by soaking in methyl alcohol. The resulting single crystals were approximately $1\times4\times4$ mm in dimension. The temperatures that were used at the various stages of this synthesis were based on phase-diagram information published by Schmitz-DuMont and Bornefeld.[3] A critical factor in the success of the synthesis was the use of KHF_2 as an initial constituent. Because of its decomposition at about 225 °C, i.e.,

$$KHF_2 \rightarrow KF + HF\uparrow,$$

HF was driven off early and fluorinated the oxide impurities and consequently purified the initial constituents.

X-ray analysis[3] shows that K_2ZnF_4 possesses the tetragonal K_2NiF_4 structure and that there are two molecules per unit cell. In addition, this analysis shows that the space group is D_{4h}^{17} with the following coordinates of equivalent positions:

000; $\frac{1}{2}\frac{1}{2}\frac{1}{2}$+		
0 0 0	$4/mmm$	Zn^{2+}
$0\ \frac{1}{2}\ 0$; $\frac{1}{2}\ 0\ 0$	mmm	F^-
0 0 Z; 0 0 $-Z$	$4mm$	$\begin{cases} F^- \\ K^+ \end{cases}$

The point symmetries as well as the ions which occupy each of the positions are also indicated here. The reported values[3] for lattice constants are $a = 4.009kX$ and $c = 13.02kX$, and for x-ray intensity measurements,[3] the Z parameters for F^- and K^+ ions were determined to be $Z_{F^-} = 0.151$ and $Z_{K^+} = 0.352$, respectively.

From these x-ray results, it is seen that the point symmetry of the Zn^{2+} ion (and thus the substituted Mn^{2+} ion in the doped K_2ZnF_4) is $4/mmm$ (or D_{4h} in the Schönflies notation). In regard to the six nearest-neighbor F^- ions shown in Fig. 1, the x-ray data show that the four planar (or type I) F^- ions are located in sites having mmm point symmetry and the two axial (or type II) F^- ions are situated in sites having $4mm$ symmetry. In addition, the data show that the nearest-neighbor Mn^{2+}-F^- interionic spacings are $\frac{1}{2}a = 2.0045kX$ for the type-I F^- ions and $0.151c = 1.97kX$ for the type-II F^- ions. Thus, there appears to be only a small departure from cubic symmetry in the nearest-neighbor environment of the Zn^{2+} ion. Moreover, a knowledge of the precise difference in these two spacings is limited by the x-ray measurements, and it is this difference that is ultimately responsible for overlap and/or covalent contributions to the axial anisotropy of a Mn^{2+} ion situated in this environment.

III. ESR EXPERIMENTAL APPARATUS

For the ESR measurements, the single crystals of K_2ZnF_4 were x-ray oriented and were attached to polystyrene rods so that either the (001) or the (100) crystallographic planes were located in the plane of the dc magnetic field when the rods were positioned along the cylindrical axis of the H_{011} mode cylindrical transmission cavity. In this arrangement either the magnetic field (produced by a Pacific Electric Motor Co. 12-in. electromagnet) could be rotated or the single crystal could be rotated in the magnetic field. For low-temperature measurements a cylindrical H_{111} mode transmission cavity was used and in the cavity the x-ray oriented single crystals were attached to the tunable plunger which formed one of the plane ends of the cavity. A Pound-stabilized klystron (operating at 24 GHz) was used for the microwave power. The output of the cavity was detected with a 1N26 silicon diode, amplified in a narrow-band 200-Hz amplifier, phase detected, and finally displayed as the first derivative of an absorption curve on an x-y recorder. The dc magnetic field was sinusoidally modulated at 200 Hz using a Helmholtz coil and the field was measured using proton and lithium nuclear resonances.

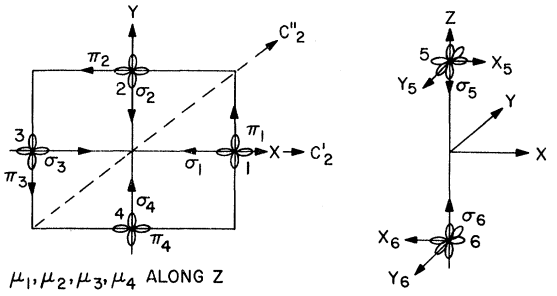

FIG. 1. Arrangement of the p_σ and p_π ligand orbitals. Labels 1, 2, 3, and 4 refer to the four equivalent F^- sites in the x-y plane and labels 5 and 6 refer to the two equivalent F^- sites on the z axis. μ_1, μ_2, μ_3, and μ_4 are π-type orbitals which are directed along the plus z axis.

IV. THEORY

In a tetragonal crystal field which exists for the ^6S ground-state Mn^{2+} ions in K_2ZnF_4, the appropriate spin Hamiltonian is[4]

$$\mathcal{H} = \mu_B g_\parallel H_Z S_Z + \mu_B g_\perp (H_x S_x + H_y S_y) + D[S_z^2 - \tfrac{1}{3}S(S+1)]$$

$$+ \tfrac{1}{180}F[35S_z^4 - 30S(S+1)S_z^2 + 25S_z^2 - 6S(S+1)$$

$$+ 3S^2(S+1)^2] + \tfrac{1}{6}a[S_x^4 + S_y^4 + S_z^4 - \tfrac{1}{5}S(S+1)(3S^2+3S-1)]$$

$$+ AS_zI_z + B(S_xI_x + S_yI_y) - g_N\mu_N\vec{H}\cdot\vec{I}, \quad (1)$$

where g_N is the splitting factor for the Mn^{55} nucleus, μ_N is the nuclear magneton, and $\vec{I}$ represents the nuclear spin operator of the Mn^{55} nucleus for which $I = \frac{5}{2}$. The symmetry about the Mn^{2+} ion in K_2ZnF_4 assures that the z axis in each of the terms in Eq. (1) coincides with the crystallographic c axis. For this equation, it is assumed that the Mn^{2+} enters the lattice substitutionally for the Zn^{2+} ions in K_2ZnF_4. Although this assumption will be experimentally verified later on, it is a reasonable one because K_2MnF_4 possesses the same crystallographic structure as K_2ZnF_4.

A. Molecular Orbitals for Mn^{2+} in K_2ZnF_4

For the purpose of obtaining ligand orbitals admixed with the central-ion d-electron orbitals, the linear-combination-of-atomic-orbitals (LCAO) method developed by Van Vleck[5-7] was used. In constructing these linear combinations, use was made of the arrangement of the p_σ and p_π ligand orbitals shown in Fig. 1. Only the F^- $2s$, $2p_\sigma$, and $2p_\pi$ orbitals were considered because these are the outermost electrons and are expected to participate in the bonding more effectively than the inner $1s$ electrons. The $2s$ electrons can be imagined to be spheres located at the six nearest-neighbor F^- sites. These sites are labeled 1, 2, 3, and 4 for the F^- ions in the x-y plane (and they are called the planar F^- ions) and 5 and 6 for the F^- ions on the z axis (called the axial F^- ions). The C_2 and C_4 symmetry axis is the z axis and the C_2' and C_2'' axes are indicated in Fig. 1. For the planar F^- ions the μ_i are π-type orbitals oriented parallel to the z axis and, for the axial F^- ions X_i and Y_i represent the two π-type orbitals. On the basis of group theory and with the use of the arrangement of ligand orbitals shown in Fig. 1, the antibonding molecular orbitals for the Mn^{2+} ion five d-electron holes are given by

$$A_{1g}:\ \Psi_{z^2}=N_1[d_{z^2}-(\lambda_{1s}/\sqrt{2})(s_5+s_6)-(\lambda_{1\sigma}/\sqrt{2})(\sigma_5+\sigma_6)-\tfrac{1}{2}\lambda_{2s}(s_1+s_2+s_3+s_4)-\tfrac{1}{2}\lambda_{2\sigma}(\sigma_1+\sigma_2+\sigma_3+\sigma_4)], \quad (2)$$

$$B_{1g}:\ \Psi_{x^2-y^2}=N_2[d_{x^2-y^2}-\tfrac{1}{2}\lambda_{3s}(s_1-s_2+s_3-s_4)-\tfrac{1}{2}\lambda_{3\sigma}(\sigma_1-\sigma_2+\sigma_3-\sigma_4)], \quad (3)$$

$$B_{2g}:\ \Psi_{xy}=N_3[d_{xy}-\tfrac{1}{2}\lambda_{1\pi}(\pi_1-\pi_2+\pi_3-\pi_4)], \quad (4)$$

$$E_g:\ \Psi_{yz}=N_4[d_{yz}-\tfrac{1}{2}\lambda_{1\mu}(Z_1+Z_2-Z_3-Z_4)-(\lambda_{2\pi}/\sqrt{2})(Y_5-Y_6)], \quad (5)$$

$$E_g:\ \Psi_{xz}=N_5[d_{xz}-\tfrac{1}{2}\lambda_{2\mu}(Z_1-Z_2-Z_3+Z_4)-(\lambda_{3\mu}/\sqrt{2})(X_5+X_6)], \quad (6)$$

where the N_i are normalizing constants, the λ are the admixture parameters, s_i refer to the s orbitals, and all the ligand orbital linear combinations are normalized. The d orbitals contained in these molecular orbitals are those which transform according to the irreducible representations indicated at the left-hand side of each equation.

B. Transferred Hyperfine Interactions

The THI can now be calculated with the aid of Eqs. (2)-(6) and with the use of the relation[8]

$$\mathcal{H}=\tfrac{8}{3}\pi g\mu_B g_F\mu_N\delta(r)(\vec{I}\cdot\vec{S}), \quad (7)$$

for the interaction between the magnetic moment of the ligand nucleus and the magnetic fields produced by the spin moments of s electrons. Here g_F refers to the F^{19} nuclear magnetic splitting factor. For interactions between the magnetic moment of the ligand nucleus and the magnetic fields produced by the spin and orbital moments of $2p$ electrons, we make use of the operator form[9] of the dipole-dipole interaction:

$$\mathcal{H}=\tfrac{2}{5}g\mu_B g_F\mu_N r^{-3}[L(L+1)(\vec{I}\cdot\vec{S})-\tfrac{3}{2}(\vec{L}\cdot\vec{I})(\vec{L}\cdot\vec{S})-\tfrac{3}{2}(\vec{L}\cdot\vec{S})(\vec{L}\cdot\vec{I})]. \quad (8)$$

From the Hamiltonians in Eqs. (7) and (8) and the molecular orbitals in Eqs. (2)-(6), we obtained the following result for the shf interaction corresponding to the type-II F^- ions:

$$\vec{I}\cdot\vec{\mathbf{A}}^{II}\cdot\vec{S}=(A_s^{II}-A_\pi^{II}-A_\sigma^{II}-A_D^{II})I_xS_x+(A_s^{II}-A_\sigma^{II}-A_D^{II}+2A_\pi^{II})I_yS_y+(A_s^{II}+2A_\sigma^{II}+2A_D^{II}-A_\pi^{II}), \quad (9)$$

where

$$A_s^{II}=\tfrac{1}{5}(f_{1s})a_s,\quad A_\sigma^{II}=(f_{1\sigma}-f_{3\mu})\tfrac{1}{5}a_p,\quad A_\pi^{II}=(f_{2\pi}-f_{3\mu})\tfrac{1}{5}a_p, \quad (10)$$

and where we have used the abbreviations

$$f_{1s}=\tfrac{1}{2}N_1^2|\lambda_{1s}|^2,\quad f_{1\sigma}=\tfrac{1}{2}N_1^2|\lambda_{1\sigma}|^2,\ldots, \quad (11)$$

$$a_s=\tfrac{8}{3}\pi g\mu_B g_F\mu_N|\psi_{2s}(0)|^2, \quad (12)$$

$$a_p=\tfrac{2}{5}g\mu_B g_F\mu_N\langle r^{-3}\rangle_{2p}. \quad (13)$$

The quantity $\psi_{2s}(0)$ is the F^- $2s$ wave function evaluated at the F^{19} nucleus and $\langle r^{-3}\rangle_{2p}$ is the expectation value with respect to the $2p$ radial wave function.

In a similar manner, we have derived the shf interaction for the planar (or type-I) F^- ions:

$$\vec{I}\cdot\vec{\mathbf{A}}^{I}\cdot\vec{S}=[A_s^I+2(A_\sigma^I+A_D^I)-A_\pi^I]I_xS_x+[A_s^I-(A_\sigma^I+A_D^I)+2A_\pi^I]I_yS_y+[A_s^I-(A_\sigma^I+A_D^I)-A_\pi^I]I_zS_z, \quad (14)$$

where

$$A_\sigma^I=(f_\sigma-f_\mu)\tfrac{1}{5}a_p,\quad A_\pi^I=(f_\pi-f_\mu)\tfrac{1}{5}a_p,\quad A_s^I=f_s\tfrac{1}{5}a_p,$$
$$f_\sigma=f_{2\sigma}+f_{3\sigma},\quad f_\mu=f_{1\mu}+f_{2\mu},\quad f_\pi=f_{1\pi}, \quad (15)$$
$$f_s=f_{2s}+f_{3s},$$

and where

$$f_{2\sigma}=N_1^2\tfrac{1}{4}|\lambda_{2\sigma}|^2,\quad f_{3\sigma}=N_2^2\tfrac{1}{4}|\lambda_{3\sigma}|^2,$$
$$f_{1\mu}=N_4^2\tfrac{1}{4}|\lambda_{1\mu}|^2,\quad f_{2\mu}=N_5^2\tfrac{1}{4}|\lambda_{2\mu}|^2,$$
$$f_{1\pi}=N_3^2\tfrac{1}{4}|\lambda_{1\pi}|^2,$$

$$f_{2s}=N_1^2\tfrac{1}{4}|\lambda_{2s}|^2,\quad f_{3s}=N_2^2\tfrac{1}{4}|\lambda_{3s}|^2. \tag{16}$$

V. EXPERIMENTAL RESULTS FOR ESR FINE AND HYPERFINE STRUCTURE

The fine and hyperfine (hf) structure can be calculated from Eq. (1). From this equation the eigenvalues (to third order in the larger spin-Hamiltonian parameters) are calculated and the resonance values of H corresponding to M, $m \leftrightarrow M-1, m$ transitions are determined from the differences $E_{M,m}-E_{M-1,m}$ in the eigenvalues. Here M and m correspond to the electronic and nuclear spin quantum numbers, respectively. For the diagonal matrix elements of the a and F terms in Eq. (1), we have

$$\begin{aligned}
\mathcal{E}_{\pm5/2}&=\tfrac{1}{2}a(1-5\varphi)+\tfrac{1}{24}F(35\cos^4\Theta-30\cos^2\Theta+3),\\
\mathcal{E}_{\pm3/2}&=-\tfrac{3}{2}a(1-5\varphi)-\tfrac{1}{8}F(35\cos^4\Theta-30\cos^2\Theta+3),\\
\mathcal{E}_{\pm1/2}&=a(1-5\varphi)+\tfrac{1}{12}F(35\cos^4\Theta-30\cos^2\Theta+3),
\end{aligned} \tag{17}$$

where the subscripts of the energies refer to the various electronic spin quantum numbers M, Θ is the angle between the c axis and the magnetic field, and $\varphi=\alpha_1^2\alpha_2^2+\alpha_2^2\alpha_3^2+\alpha_1^2\alpha_3^2$, in which the α's are the direction cosines of the magnetic field with respect to the a, b, and c crystal axes in K_2ZnF_4. The a-term energies in Eq. (17) were calculated by Kronig and Bouwkamp[10] and the F-term contributions to the ESR resonance fields were obtained by Bleaney and Trenam.[11] As will be seen later, the a and F parameters are small so that it is only necessary to compute the first-order perturbation energies for these parameters. However, it is necessary to go to higher order in the perturbation calculations for the other parameters.

A. Analysis of [001] Spectrum

For measurements with H parallel to the c axis, Eqs. (1) and (17) yield the relations[12,13] for the resonance values of H corresponding to M, $m \leftrightarrow M-1$, m transitions:

$$H_{5/2,m}=H_0-4D-2(a+\tfrac{2}{3}F)-Am-(B^2/2H_0)(\tfrac{35}{4}-m^2+4m)$$
$$+(B^2D/2H_0^2)[12(\tfrac{35}{4}-m^2)+8m]-(B^2A/2H_0^2)[4(\tfrac{35}{2}-3m^2)+m(m^2-\tfrac{17}{4})], \tag{18}$$

$$H_{3/2,m}=H_0-2D+\tfrac{5}{2}(a+\tfrac{2}{3}F)-Am-(B^2/2H_0)(\tfrac{35}{4}-m^2+2m)$$
$$+(B^2D/2H_0^2)[6(\tfrac{35}{4}-m^2)-10m]-(B^2A/2H_0^2)[2(\tfrac{35}{2}-3m^2)+m(m^2-\tfrac{53}{4})], \tag{19}$$

$$H_{1/2,m}=H_0-Am-(B^2/2H_0)(\tfrac{35}{4}-m^2)-(8B^2D/H_0^2)m-(B^2A/2H_0^2)[m(m^2-\tfrac{65}{4})], \tag{20}$$

$$H_{-1/2,m}=H_0+2D-\tfrac{5}{2}(a+\tfrac{2}{3}F)-Am-(B^2/2H_0)(\tfrac{35}{4}-m^2-2m)$$
$$+(B^2D/2H_0^2)[6(m^2-\tfrac{35}{4})-10m]-(B^2A/2H_0^2)[2(3m^2-\tfrac{35}{2})+m(m^2-\tfrac{53}{4})], \tag{21}$$

$$H_{-3/2,m}=H_0+4D+2(a+\tfrac{2}{3}F)-Am-(B^2/2H_0)(\tfrac{35}{4}-m^2-4m)$$
$$+(B^2D/2H_0^2)[12(m^2-\tfrac{35}{4})+8m]-(B^2A/2H_0^2)[4(3m^2-\tfrac{35}{2})+m(m^2-\tfrac{17}{4})], \tag{22}$$

where $H_0=h\nu/g_\parallel\mu_B$ and the parameters D, a, F, A, and B are now divided by $g_\parallel\mu_B$.

In the ESR spectrum for $H\parallel[001]$ direction, the number of possible lines resulting from $\Delta M=\pm1$, $\Delta m=0$ transitions is $(2S+1)(2I+1)(15)=540$, where the factor of 15 arises from the shf interactions which will be discussed in Sec. VI A. Because of the large number of lines there is considerable overlapping of the ESR spectrum. For this reason it was necessary to choose lines for which the overlapping effect did not occur or was negligibly small so that the position of these lines could be accurately determined in the ESR measurements.

The spectroscopic splitting factor $g_\parallel$ was determined from the measurements of $H_{-3/2,5/2}$ and $H_{5/2,-5/2}$ for which there is no overlapping of lines. The deduced value for $g_\parallel$ is shown in Table I. Since it is well established that the quantity A is negative, then the term $-Am$ will yield hf lines which will occur at the highest values of H when $m=\frac{5}{2}$ and at the lowest values of H when $m=-\frac{5}{2}$. Using this information, we have determined the sign of D to be positive.

From the measured values of $H_{-3/2,5/2}$, $H_{5/2,-5/2}$, $H_{-1/2,5/2}$, $H_{3/2,-5/2}$, $H_{-1/2,3/2}$, and $H_{3/2,-3/2}$ we have deduced the quantities $g_\parallel$, A, D, and $a+\frac{2}{3}F$. The values for $g_\parallel$, A, and D are shown in Table I and for the latter quantity, we find

$$a+\tfrac{2}{3}F=6.9\times10^{-4}\ \text{cm}^{-1}. \tag{23}$$

TABLE I. Values of fine and hf structure parameters for $K_2ZnF_4:Mn^{2+}$. The quantities A, B, D, a, and F are in units of 10^{-4} cm^{-1}.

$g_{\parallel}$	2.0030 ± 0.0001
$g_{\perp}$	2.0028 ± 0.0002
A	-88.7 ± 0.1
B	-89.3 ± 0.2
D	36.0 ± 0.2
a	5.6 ± 0.3
F	1.9 ± 0.6

It was necessary to analyze the spectrum for H in the [110] direction in order to obtain values for a and F separately.

B. Analysis of [110] Spectrum

The ESR spectrum for H directed along the [110] direction can contain as many as 540 lines corresponding to $\Delta M = \pm 1$, $\Delta m = 0$ transitions. Therefore, it was again necessary to confine the analysis to the experimentally measured ESR lines for which the overlapping with other lines was either zero or minimal. For an analysis of these measurements, we used the relations[11,13] for the resonance values of H as calculated to second order in perturbation theory. These relations, which are valid for measurements in the (001) plane, are

$$H_{5/2,m} = H_0 + 2D + D^2/H_0 - 2pa - \tfrac{1}{2}F - Bm - [(A^2+B^2)/4H_0](\tfrac{35}{4} - m^2 + 4m), \quad (24)$$

$$H_{3/2,m} = H_0 + D - \tfrac{5}{4}D^2/H_0 + \tfrac{5}{2}pa + \tfrac{5}{8}F - Bm - [(A^2+B^2)/4H_0](\tfrac{35}{4} - m^2 + 2m), \quad (25)$$

$$H_{1/2,m} = H_0 - 2D^2/H_0 - Bm - [(A^2+B^2)/4H_0] \times (\tfrac{35}{4} - m^2), \quad (26)$$

$$H_{-1/2,m} = H_0 - D - \tfrac{5}{4}D^2/H_0 - \tfrac{5}{2}pa - \tfrac{5}{8}F - Bm - [(A^2+B^2)4H_0](\tfrac{35}{4} - m^2 - 2m), \quad (27)$$

$$H_{-3/2,m} = H_0 - 2D + D^2/H_0 + 2pa + \tfrac{1}{2}F - Bm - [(A^2+B^2)/4H_0](\tfrac{35}{4} - m^2 - 4m), \quad (28)$$

where $H_0 = h\nu/g_{\perp}\mu_B$. Here

$$p = 1 - 5\varphi = -\tfrac{1}{4} \text{ for } H \parallel [110]$$
$$= 1 \quad \text{for } H \parallel [100]. \quad (29)$$

Choosing again those transitions for which the overlapping with other ESR lines is minimal, we obtain from the measurements of $H_{5/2,5/2}$, $H_{-3/2,-5/2}$, and $H_{-1/2,-5/2}$ the values of $g_{\perp}$ and B shown in Table II and the relation

$$a - F = 3.7 \times 10^{-4} \text{ cm}^{-1}. \quad (30)$$

Combining Eq. (30) with Eq. (23) yields the values of a and F shown in Table II. As a check on the value of the a value thus determined, we have performed measurements of $H_{-1/2,-5/2}$ with H directed along a [100] direction. Using Eqs. (27) and (29), we find

$$[H_{-1/2,-5/2}]_{[110]} - [H_{-1/2,-5/2}]_{[100]} = \tfrac{25}{8}a,$$

and from the experimental results on the difference in the left-hand side of this equation, we obtain $a = 5.6 \times 10^{-4}$ cm^{-1}, in agreement with the independently determined value shown in Table I.

VI. SUPERHYPERFINE STRUCTURE

A. Superhyperfine Structure for H in [001] Direction

The shf structure for H in the [001] direction results from the interaction Hamiltonians given in Eqs. (9) and (14). In order to interpret the observed shf spectrum one has to sum over all the interactions from type-I and type-II fluorines. Thus, we must add to the spin Hamiltonian the term

$$\mathcal{H}(F^{19}) = \sum_{i=1}^{4} \vec{I}_i \cdot \overleftrightarrow{A}^{I} \cdot \vec{S} + \sum_{i=5}^{6} \vec{I}_i \cdot \overleftrightarrow{A}^{II} \cdot \vec{S}, \quad (31)$$

where the first sum is over the four type-I fluorines and the second sum is over the two type-II fluorines. In Eq. (31) a typical term for a type-I fluorine is given by Eq. (15) and a term for the second sum is given by Eq. (9). Consider now the shf interaction terms involving S_x or S_y in Eq. (9) or (15). These terms will produce negligibly small effects because they yield only off-diagonal contributions when $H \parallel Z$ and consequently are of the order of $A_s^2/H_0 \approx 0.05$ G. In the approximation where these terms are neglected, Eq. (31) reduces to

$$\langle M, m_F | \mathcal{H}(F^{19}) | M, m_F \rangle = (m_F^{(1)} + m_F^{(2)} + m_F^{(3)} + m_F^{(4)}) \times [A_s^I - (A_\sigma^I + A_D^I) - A_\pi^I] M + (m_F^{(5)} + m_F^{(6)}) \times [A_s^{II} + 2A_\sigma^{II} + 2A_D^{II} - A_\pi^{II}] M, \quad (32)$$

TABLE II. shf parameters for $K_2ZnF_4:Mn^{2+}$ in units of 10^{-4} cm^{-1}.

	A_s	A_σ[a]	A_π[a]
Type I	18.1 ± 0.2	0.4 ± 0.2	$\approx 0 \pm 0.2$
Type II	14.9 ± 0.4	$A_\sigma^{II} - \tfrac{1}{2}A_\pi^{II} = 0.3 \pm 0.2$	...

[a]Based on the calculated values $A_D^I = 3.3$ G and $A_D^{II} = 3.0$ G. For self-consistency, the interionic spacings used in these calculations were determined from the experimental values of A_s^I and A_s^{II} assuming the admixture parameter $\lambda \cong S$, where S is the overlap integral. For details see Refs. 2 and 14.

where $m_F^{(i)}$ is the F^{19} spin quantum number of the ith F^{19} nucleus as defined in Fig. 1. Since each F^{19} nucleus is independent of one another, the sum over the nuclear spin quantum number in the first term of Eq. (31) can take on $2(4I_F)+1=5$ values and the sum in the second term can take on $2(2I_F)+1=3$ values. Thus the first term in Eq. (32) will split each of the Mn^{2+} hf lines into five shf lines and the second term in this equation will split each of the shf lines into three lines, so that each hf line will be split into 15 lines when $H \parallel Z$.

The spectrum shown in Fig. 2 is a diagram of the 15-line spectrum corresponding to the split $H_{-3/2,5/2}$ hf line. This diagram is based on the results of the following analysis of the observed spectrum, a portion of which is indicated by the solid curve of Fig. 3. The numbers above each of the lines in Fig. 2 represent the relative amplitudes of the shf lines and are statistical weights which are based on the number of combinations of the $m_F^{(i)}$ that will produce a specific total component. Due to the overlapping of the shf lines (as shown in Fig. 3), it was necessary to fit the experimental spectrum in Fig. 3 by the superposition of Lorentzian lines. Lorentzian line shapes were chosen because they produce the best fit of the spectrum.

The observed 15-line shf spectrum was fit by an iteration process involving the superposition of 15 derivative Lorentzian lines with three adjustable parameters, namely, the linewidth and the two bracketed quantities on the right side of Eq. (32). The results of the best fit are shown by the circles in Fig. 3 and the deduced values for the bracketed quantities in Eq. (32) are

$$A_S^I - A_\sigma^I - A_D^I - A_\pi^I = 15.7 \pm 0.2 \text{ G}, \tag{33}$$

$$A_S^{II} + 2A_\sigma^{II} + 2A_D^{II} - A_\pi^{II} = 22.5 \pm 0.2 \text{ G}. \tag{34}$$

One can calculate A_D^I and A_D^{II} (which represent the classical magnetic dipole-dipole interaction) from

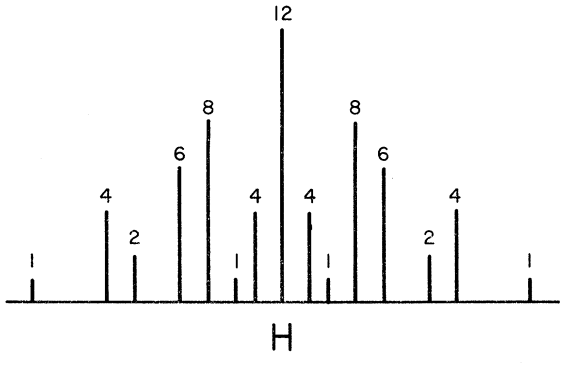

FIG. 2. Diagram of the 15-line shf spectrum of the split $H_{-3/2,5/2}$ hf line, for $H \parallel [001]$.

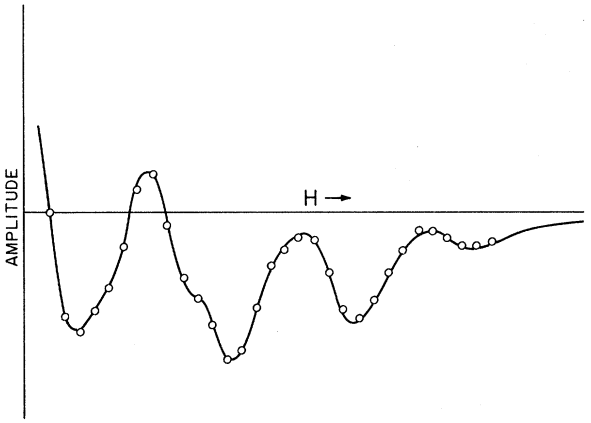

FIG. 3. shf spectra for the [001] measurements of the $M=-3/2$, $m=5/2 \rightarrow M=-5/2$, $m=5/2$ transition in $K_2ZnF_4:Mn^{2+}$. The solid line corresponds to experimental data and the circles are theoretical points.

the interionic spacings in K_2ZnF_4. However, it was necessary to perform measurements with $H \parallel [110]$ in order to evaluate separately the individual shf tensor components in Eqs. (33) and (34).

B. Superhyperfine Structure for H in [110] Direction

For the analysis of the measurements with $H \parallel [110]$ direction, the xx and yy components of the A^I and A^{II} shf tensors can be transformed to axes parallel and perpendicular to the [110] direction. Letting ζ be the parallel axis and η be the perpendicular axis (in the x-y plane), the shf interaction in Eq. (9) can be written

$$\vec{I}\cdot\vec{\vec{A}}^{II}\cdot\vec{S} \cong (A_s^{II} + \tfrac{1}{2}A_\pi^{II} - A_D^{II} - A_\sigma^{II}) I_\zeta S_\zeta + \tfrac{3}{2}A_\pi^{II} I_\eta S_\zeta$$

$$= A_{\zeta\zeta}^{II} I_\zeta S_\zeta + A_{\eta\zeta}^{II} I_\eta S_\zeta, \tag{35}$$

where off-diagonal terms in S are again neglected for reasons similar to those given in Sec. VI A. Similarly, the transformed shf tensor for the type-I fluorines is

$$\vec{I}\cdot\vec{\vec{A}}^{I}\cdot\vec{S} \cong (2A_s^I + A_D^I + A_\sigma^I + A_\pi^I) I_\zeta S_\zeta + \tfrac{3}{2}(A_D^I + A_\sigma^I - A_\pi^I) I_\eta S_\zeta$$

$$= A_{\zeta\zeta}^I I_\zeta S_\zeta + A_{\eta\zeta}^I I_\eta S_\zeta . \tag{36}$$

In Eqs. (35) and (36), the second term (proportional to I_η) can be considered as being proportional to an effective field perpendicular to the axis of quantization ζ. When these terms are comparable in magnitude to the first term, it is necessary to quantize[15] along a direction corresponding to the resultant of the effective fields that exist for the F^{19} nucleus. In particular, the quantity A_D^I in the second term of Eq. (36) is comparable to the largest quantities in the first term. Thus for a F^{19}

nucleus of type I, the total Hamiltonian that must be used is

$$\mathcal{H}^{\mathrm{I}} = (A^{\mathrm{I}}_{\xi\xi} M - g_{\mathrm{F}}\,\mu_N H_0)\, I_\xi + A^{\mathrm{I}}_{\eta\xi} M I_\eta\,, \tag{37}$$

in which the Zeeman energy of the F^{19} nucleus is included. On the basis of Eq. (37) we note that there are effective fields along the ξ and η axes. Consequently, if ξ' is the direction of the resultant field we have

$$\mathcal{H}^{\mathrm{I}} = -I_{\xi'}\,[(A^{\mathrm{I}}_{\xi\xi} M - g_{\mathrm{F}}\,\mu_N H_0)^2 + (A^{\mathrm{I}}_{\eta\xi})^2 M^2]^{1/2}, \tag{38}$$

and the angle between ξ and ξ' is given by

$$\tan\theta = \frac{A^{\mathrm{I}}_{\eta\xi} M}{A^{\mathrm{I}}_{\xi\xi} M - g_{\mathrm{F}}\,\mu_N H_0}\,.$$

Taking the matrix element $\langle m_{\mathrm{F}}^{(i)} | \mathcal{H}^{\mathrm{I}} | m_{\mathrm{F}}^{(i)} \rangle$, we obtain the energy

$$\mathcal{E}^{\mathrm{I}}_M = -\sum_{i=1}^{4} m_{\mathrm{F}}^{(i)}\,[(A^{\mathrm{I}}_{\xi\xi} M - g_{\mathrm{F}}\,\mu_N H_0)^2 + (A^{\mathrm{I}}_{\eta\xi})^2 M^2]^{1/2}\,, \tag{39}$$

where $m_{\mathrm{F}}^{(i)}$ now is the quantum number for which ξ' is the axis of quantization. Similarly, using Eqs. (35) we obtain the energy for the type-II fluorines:

$$\mathcal{E}^{\mathrm{II}}_M = -\sum_{i=5}^{6} m_{\mathrm{F}}^{(i)}\,[(A^{\mathrm{II}}_{\xi\xi} M - g_{\mathrm{F}}\,\mu_N H_0)^2 + (A^{\mathrm{II}}_{\eta\xi})^2 M^2]^{1/2}\,. \tag{40}$$

One can obtain from Eqs. (39) and (40) the positions of the shf spectrum for $H \parallel [110]$. For this purpose, it is necessary to take the differences $\mathcal{E}^{\mathrm{I}}_{M+1} - \mathcal{E}^{\mathrm{I}}_M$ and $\mathcal{E}^{\mathrm{II}}_{M+1} - \mathcal{E}^{\mathrm{II}}_M$ corresponding to $\Delta M = \pm 1$ transitions. Since there are two contributions to shf splitting [arising from Eqs. (39) and (40)], a 15-line shf spectrum should exist. The experiments for $H \parallel [110]$ yielded such a spectrum and values for bracketed quantities in Eqs. (39) and (40). These data were analyzed by using the method involving the superposition of Lorentzian lines and a best-fit procedure similar to that used for the [001] data analysis discussed in Sec. VI A.

The shf resonance lines which were used in the [110] data analysis were those corresponding to the $H_{-3/2,5/2}$ and $H_{5/2,5/2}$ hf structure lines. This analysis yielded the values

$$A^{\mathrm{II}}_s - A^{\mathrm{II}}_\sigma - A^{\mathrm{II}}_D + \tfrac{1}{2} A^{\mathrm{II}}_\pi = 12.6 \pm 0.4\ \mathrm{G}\,, \tag{41}$$

$$\tfrac{1}{2}[2A^{\mathrm{I}}_s + A^{\mathrm{I}}_D + A^{\mathrm{I}}_\sigma + A^{\mathrm{I}}_\pi] = 21.2 \pm 0.2\ \mathrm{G}\,, \tag{42}$$

$$\tfrac{3}{2}[A^{\mathrm{I}}_D + A^{\mathrm{I}}_\sigma - A^{\mathrm{I}}_\pi] = 5.4 \pm 0.2\ \mathrm{G}\,. \tag{43}$$

Using the calculated values of $A^{\mathrm{I}}_D = 3.3$ G, the results $A^{\mathrm{I}}_s + 2A^{\mathrm{I}}_D + 2A^{\mathrm{I}}_\sigma - A^{\mathrm{I}}_\pi = 26.8 \pm 0.4$ G from measurements with $H \parallel [100]$, and Eqs. (33) and (42), we determined the values of A^{I}_s, A^{I}_σ, and A^{I}_π shown in Table II. Also, using $A^{\mathrm{II}}_D = 3.0$ G and Eqs. (34) and (43), we obtained the values of A^{II}_s and $A^{\mathrm{II}}_\sigma - \frac{1}{2} A^{\mathrm{II}}_\pi$ shown in Table II.

VII. DISCUSSION

The present investigation has yielded values for the fine, hf, and shf spin-Hamiltonian parameters for Mn^{2+} in a tetragonal environment. From the shf parameters in Table II the fraction of unpaired spin densities in the $2s$ and $2p$ F^- orbitals can be calculated using the F^- values[16] $|\psi(0)|^2 = 10.7$ a.u. and $\langle r^{-3} \rangle_{2p} = 6.45$ a.u. Thus, we obtain from Eqs. (10) and (15) the fractions $f_{2s} + f_{3s} = 0.60\%$, $f_{2\sigma} + f_{3\sigma} - f_{1\mu} - f_{2\mu} = 0.5\%$, and $f_{1\pi} - f_{1\mu} - f_{2\mu} = 0\%$ for type-I fluorines, and $f_{1s} = 0.50\%$ and $f_{1\sigma} - f_{3\mu} \cong 0.4\%$ for type-II fluorines. These values represent fractions of unpaired spin densities for an electron hole[15,17] in the $2s$, $2p_\sigma$, or $2p_\pi$ orbitals. A comparison of the values for A^{I}_s and A^{II}_s in Table II indicates (using overlap-covalency considerations) that the Mn^{2+}-F^- distance for the type-I F^- ions is smaller than that for the type-II F^- ions. Consequently, one would expect a similar variation in the corresponding distances determined from the x-ray data.[3] However, the interionic distance for the type-I F^- ions appears to be the larger of the two on the basis of the x-ray data. Although it is not expected that the lattice geometry in the vicinity of the Mn^{2+} ion is in exact correspondence with that in the vicinity of the Zn^{2+} ion, one would expect the Mn^{2+}-F^- distances to vary qualitatively in a similar manner for both ions in the same host lattice.

The experimental results on the shf tensor components can be used in conjunction with theory (involving spin-orbit and intraionic spin-spin interactions) to determine the electronic overlap contributions to the independently measured D parameter, the quantity which is responsible for the axial anisotropy of Mn^{2+}. Such an application of these experimental results will appear[14] in a forthcoming paper by the present author.

ACKNOWLEDGMENT

The author wishes to express his gratitude to R. A. Becker for assistance in the single-crystal synthesis.

*Based on a portion of a Ph. D. thesis submitted to the Physics Department, The American University, Washington, D. C.

[1] J. Owen and K. W. H. Stevens, Nature 171, 836 (1953).

[2] J. Owen and J. H. M. Thornley, Rept. Progr. Phys. 29, 675 (1966).

[3] O. Schmitz-DuMont and H. Bornefeld, Z. Anorg. Allgem. Chem. 287, 120 (1956).

[4] W. Low, *Paramagnetic Resonance in Solids* (Academic, New York, 1960).

[5] J. H. Van Vleck, J. Chem. Phys. 3, 803 (1935).

[6]J. H. Van Vleck, J. Chem. Phys. 3, 807 (1935).
[7]J. H. Van Vleck and A. Sherman, Rev. Mod. Phys. 7, 167 (1935).
[8]E. Fermi, Z. Physik 60, 320 (1930).
[9]A. Abragam and M. H. L. Pryce, Proc. Roy. Soc. (London) A205, 135 (1951).
[10]E. de L. Kronig and C. J. Bouwkamp, Physica 6, 290 (1939).
[11]B. Bleaney and R. S. Trenam, Proc. Roy. Soc. (London) A205, 336 (1951).
[12]V. J. Folen, Phys. Rev. 139, A1961 (1965).
[13]B. Bleaney and D. J. E. Ingram, Proc. Roy. Soc. (London) A205, 336 (1951).
[14]V. J. Folen (unpublished).
[15]A. M. Clogston, J. P. Gordon, V. Jaccarino, M. Peter, and L. R. Walker, Phys. Rev. 117, 1222 (1960).
[16]S. Sugano and Y. Tanabe, J. Phys. Soc. Japan 20, 1155 (1965).
[17]R. E. Watson and A. J. Freeman, Phys. Rev. 134, A1526 (1964).

PHYSICAL REVIEW B VOLUME 6, NUMBER 5 1 SEPTEMBER 1972

Nuclear Magnetic Resonance in the LaX_3 Intermetallic Compounds*

L. B. Welsh
Department of Physics, Northwestern University, Evanston, Illinois 60201

and

A. M. Toxen and R. J. Gambino
IBM Watson Research Center, Yorktown Heights, New York 10598

(Received 23 February 1972)

The La^{139} nuclear-magnetic-resonance (NMR) Knight shift and spin-lattice relaxation time (T_1) in $LaPb_3$ were measured from 1.5 to 300 °K. The isotropic and anisotropic Pb^{207} Knight shifts were measured at 1.5, 4.2, and 77 °K and T_1 was measured at 1.55 °K. Also presented are measurements of the La T_1 in $LaIn_3$ from 1.5 to 300 °K which are more complete than previously reported. These measurements are compared with previously reported measurements for $LaSn_3$. The La^{139} Knight shift (+0.010% at 4.2 °K) in $LaPb_3$ has a temperature dependence roughly five times that found in $LaSn_3$ and $LaIn_3$ even though the bulk susceptibility is considerably smaller. For $LaPb_3$, the La T_1T product is nearly temperature independent (T_1T = 0.59 sec °K at 4.2 °K) and is about half that found in $LaSn_3$. For $LaIn_3$, T_1T increases by 50% between 1.5 and 300 °K and has a temperature dependence similar to $LaSn_3$. The isotropic and anisotropic Pb Knight shifts (K_{iso} = +0.70% and $3K_{ax}$ = +0.43% at 4.2 °K) are nearly temperature independent. The Pb relaxation time in $LaPb_3$ ($T_1T = 63\times10^{-4}$ sec °K) is about four times faster than in Pb metal, indicating a larger s-contact contribution than in Pb metal and a large negative Knight-shift component. The La NMR and bulk-susceptibility data are partitioned using the customary approximation for transition metals. We find the results for $LaIn_3$ and $LaSn_3$ are quite similar suggesting that in both these materials the La d-orbital susceptibility is much larger than the d-spin susceptibility and that exchange-enhancement effects are probably not important. For $LaPb_3$, d-orbital effects are less important than the d-spin contributions. In all three compounds the La d-spin contributions to the NMR properties and the bulk susceptibility are of similar magnitude.

I. INTRODUCTION

The LaX_3 intermetallic compounds (X = Sn, In, Pb, Tl, etc.) have been the subject of a number of recent experimental and theoretical studies which have attempted to determine their magnetic and superconducting properties.[1–5] Because of their interesting properties, band-structure calculations for some of these compounds have also received considerable attention.[6,7] In this paper we present the results of nuclear-magnetic-resonance (NMR) studies of these compounds which allow a comparison of the microscopic behavior of the band electrons at the La and X sites in different compounds and a determination of the various spin and orbital contributions to their NMR and bulk magnetic properties.

The most intriguing property of the LaX_3 intermetallic compounds is the coexistence of a fairly high superconducting transition temperature T_c and a large temperature-dependent paramagnetic susceptibility χ for some of these compounds. Several authors[8–10] have shown that for alloys of these compounds both T_c and χ vary radically with changing electron/atom (e/a) ratio and that maximum values of T_c and χ occur at nearly the same e/a ratios. For $LaSn_3$, $LaPb_3$, and $LaIn_3$ the superconducting transition temperatures are 6.45, 4.05, and 0.68 °K, respectively,[2,4] and the susceptibilities at 4.2 °K are 3.3